Fast and Accurate Analytical Thermal Modeling for Planar PCB Magnetic Components

Lucia Clavero Ordonez, *Graduate Student Member, IEEE*, Alberto Delgado Exposito, *Member, IEEE*, Pedro Alou Cervera, *Member, IEEE*, Miroljub Bakic, and Thiwanka Wijekoon, *Senior Member, IEEE*

***Abstract*—The exploitation of PCB integrated magnetic components in the high power field brings new challenges due to the compactness of the design and the poor thermal performance of components using standard PCB technology. In this work, a thermal modeling approach is proposed, which is suitable for optimization based design of planar PCB magnetic components. The targets are high accuracy, low computation time, and easy implementation. The results show an accuracy comparable to finite element simulations, with average absolute error of 1.3 °C with respect to measurement, while the computation time is 13 times shorter than simplified finite element simulations. The equations are purely analytical, i.e., no measurements or simulations are needed to obtain the involved parameters. The structure of the model enables easy and fast generation of PCB geometries, with the possibility to make a parametric sweep of any variable. The model has been verified with finite element simulations and experimental measurements for a wide range of operating conditions, including dc and ac excitation.**

***Index Terms*—Finite elements, PCB transformer, planar magnetics, thermal model, thermal network.**

I. Introduction

The trend of low profile—PCB integrated magnetic components has led to power density improvement and reduction of the cost and complexity of serial production in low power applications (i.e., < 1 kW). The interest for this technology is growing increasingly in high power applications, chasing for equivalent benefits. However, the compactness of these components, together with the use of insulating materials with low thermal conductivity (such as FR4 materials typically used in PCB), results in poor thermal performance, which limits their implementation at high power applications [1].

For such high power applications, heat extraction becomes critical to ensure long term reliability, and the potential temperature variations must be considered in the design stage, rather than just for verification. Temperature estimations based on generalized experimental thermal resistances are useful as a starting point for size approximation. These formulas can be found in literature [2], standards [3], or in the information provided by manufacturers.

The design procedure for magnetic components can be complex, and usually several possible configurations are compared in order to find the most optimal design for an application. Therefore, simplified 1-D and 2-D thermal models are extensively used to provide a fast approximation of the temperature rise under operating conditions. Some of these models are based on the solution of the heat transfer differential equations [4]. However, the most commonly used are thermal networks, which analyze the relation between heat flow and temperature in a material as an analogy of the relation between current and voltage in an electric circuit [5], [6], [7].

In these thermal networks, the opposition against heat flow through a certain path is modeled by a thermal resistance. The reduction of these models to 1-D or 2-D in space is justified by the presence of lower thermal resistance paths, either because of the use of high thermal conductivity materials (such as copper) or due to proximity to heat dissipators (as heat sinks, or cooling fluids).

Measurement or simulation-based parameters are included in [5] and [6] to reduce inaccuracies, with the consequent expense in time and automation. The authors in [8] and [9] consider heat flow paths in different dimensions in space, but reducing them to an equivalent 1-D circuit. The neglected heat paths and the use of lower resolution circuits in these models affect the accuracy of the results. In [9], shape factors are used to calculate the convection coefficients, and consideration of the thermal surface impedance variation with frequency proofs to improve accuracy. More complex networks can be built considering 3-D elements as in [10], [11], and [12], but the simplicity and speed of the model are compromised.

When accurate results are required, as for verification of the design previous to final production, finite element (FE) tools are employed. The accuracy in this case depends on mesh refinement and adequate setting of boundary conditions, leading

Manuscript received 20 October 2022; revised 25 January 2023; accepted 13 March 2023. Date of publication 20 March 2023; date of current version 20 April 2023. This work was supported by Huawei Technologies Duesseldorf GmbH. Recommended for publication by Associate Editor R. Hui. *(Corresponding author: Lucia Clavero Ordonez.)*

Lucia Clavero Ordonez is with the Universidad Politécnica de Madrid, Escuela Técnica Superior de Ingenieros Industriales, 28006 Madrid, Spain, and also with the Huawei Technologies Duesseldorf GmbH, Nuremberg Research Center, 90449 Nuremberg, Germany (e-mail: lucia.clavero.ordonez@alumnos.upm.es).

Alberto Delgado Exposito and Pedro Alou Cervera are with the Universidad Politécnica de Madrid, Escuela Técnica Superior de Ingenieros Industriales, 28006 Madrid, Spain (e-mail: a.delgado@upm.es; pedro.alou@upm.es).

Miroljub Bakic and Thiwanka Wijekoon are with the Huawei Technologies Duesseldorf GmbH, Nuremberg Research Center, 90449 Nuremberg, Germany (e-mail: Miroljub.Bakic@huawei.com; thiwanka.wijekoon@ieee.org).

Color versions of one or more figures in this article are available at https://doi.org/10.1109/TPEL.2023.3259064.

Digital Object Identifier 10.1109/TPEL.2023.3259064

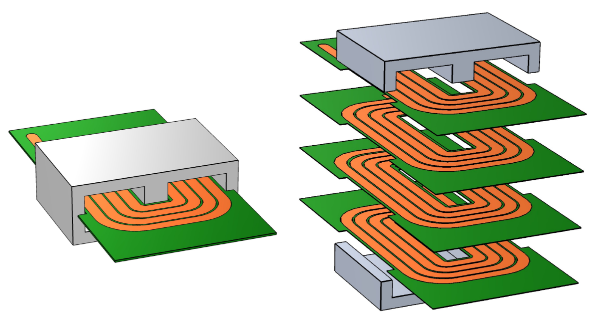

Fig. 1. Representation of the layered structure of a PCB winding in planar transformers. Left: Planar transformer example. Right: Exploited vision of the PCB layers.

to results close to measurement when the simulated model fairly represents real conditions.

FE can also be used to optimize the operating conditions of a component. For this purpose, the model consists of a linearization of the thermal resistance for the range of interest. The model can be obtained applying the superposition concept to the heat sources [13] or training an artificial intelligence (AI) based model with different losses and boundary conditions [14]. These are highly accurate models but they cannot be used to analyze geometric variations and it takes several FE simulation attempts to build them accurately.

The state of the art models can be divided into fast simplified models and accurate models. Nevertheless, the ideal model for optimization of a component would be both fast and accurate, specially when the analyzed variable (temperature rise in the case which is the interest of this article) is critical for the component operation.

The main contribution of this article was presented in [15] in a general approach. In this article, a comprehensive explanation of the model is covered, as well as a deeper study on speed and accuracy. This model can achieve both speed and accuracy for the case of PCB transformers and inductors. The following assumptions have been considered in this work based on the characteristics of PCB technology:

1) *2-D Geometry approximation:* The relevant geometrical information in a PCB component is almost purely contained in the 2-D plane containing each of the layers, represented in Fig. 1. A model defining precisely the geometry in the planes of interest will sufficiently represent the real 3-D component.
2) *Layered structure:* The aforementioned 2-D planes form the layers of the PCB component. The layers containing copper are separated by insulation layers and connected through vias.
3) *Thin plate approximation:* The ratio between the flat surface and the PCB thickness is very large. Convection in the PCB sides due to either natural or forced cooling techniques can be neglected.
4) *Power loss uniformity:* High frequency effects cause a nonuniform distribution of current density flowing inside the windings. The higher currents in the borders of the tracks increase the losses, which are not evenly distributed. However, due to high thermal conductivity of copper, the power loss distribution inside each layer can be considered uniform for thermal analysis.

The rest of this article is organized as follows. In Section II, the theory of heat transfer and the specific application considered in this work for planar magnetic components is presented. In Section III, the loss model used for validation of the proposed thermal model is exposed, focusing on the interdependence between loss and temperature. The model assembly and solution are explained in Section IV, considering the structure of the model based on the exposed assumptions, the calculation of parameters, and how the results are obtained. The model is verified in Section V through comparison with FE simulations and thermal camera measurements for several specimens of transformers and inductors. Finally, the conclusions are discussed in Section VI.

II. Heat Transfer Equations for Magnetic Components

Heat transfer mechanisms are divided in conduction, convection, and radiation [16], [17]. In thermal networks, the opposition of a path to heat flow is represented by a thermal impedance, formed by resistances and capacitances [18], [19]. The resistances determine the behavior of the component in steady state, while the capacitances model the thermal inertia.

Components with high thermal inertia, such as magnetic components, behave as an overdamped system against variations in the applied power. Thus, the most critical condition under stable operation is the steady state, where the component reaches the maximum temperature. The presented model studies the steady state, so only the real part of the thermal impedance is considered.

A. Conduction

In a magnetic component, conduction is the predominating process inside the winding, due to high thermal conductivity of copper (around 400 W/mK). In PCB components, the windings are embedded in an insulating material, which usually presents very low thermal conductivity (0.3 W/mK for typically used FR4 materials [7]).

The heat flow q along a path due to conduction is expressed in (1), where q is the heat flow, k the thermal conductivity of the material, A the cross-sectional surface of the considered path, and L the length of the path [16]. This equation is expressed in the form of a thermal resistance R_{cond} in (2):

$$q = \frac{kA}{L}\Delta T \tag{1}$$

$$R_{\text{cond}} = \frac{\Delta T}{q} = \frac{L}{kA}. \tag{2}$$

B. Convection

Convection occurs when a fluid is present. The quality of the cooling technique is marked by the fluid properties, the convective surface and the speed and temperature of the fluid flow [16]. This is accounted by the denominated heat transfer coefficient h in (3). The thermal resistance associated with

convection, R_{conv} in (4), is calculated analogously to conduction

$$q = hA\Delta T \tag{3}$$

$$R_{\text{conv}} = \frac{1}{hA}. \tag{4}$$

The heat transfer coefficient depends on the fluid properties in the proximity of the refrigerated surface, which vary with temperature. Experimental correlations for different surface shapes and orientations can be used to estimate the heat transfer coefficient of each surface of the object, evaluating the fluid properties at the film temperature [16], [17]. The scope of these correlations covers simple geometries, which makes them suitable for PCB components, where most surfaces can be considered as flat plates. Nevertheless, these correlations assume that the surfaces are either isothermal or isoflux, which often does not occur in real conditions.

State-of-the-art thermal networks commonly evaluate the mentioned correlations at the average temperature of the surfaces, leading to lower accuracy. In this work, this problem is overcome by evaluating the equations at the node temperature, while considering the area and geometrical aspect ratio of the whole surface. This way the nonuniformities in the temperature distribution are taken into account.

The dependence of the heat transfer coefficient on temperature is inherited by the corresponding thermal resistances, which means the solution of a thermal resistance based method is not straightforward. This will be addressed in Section IV.

C. Radiation

The radiation phenomenon is originated by the reduction of internal energy stored in a form of matter. However, the presence of matter is not required for its transport.

The heat exchange between two surfaces due to radiation can be analyzed through a view factor, which defines the fraction of the radiation emitted by one surface that is intercepted by the other surface. As for the heat transfer coefficient, experimental formulas exist to estimate the view factor for simple geometries [16].

A network approach can also be used to represent the radiation balance in an enclosure. However, the represented magnitudes in a radiation network are different to those in the previously described thermal network, so they cannot be merged directly.

A common simplification of the problem is to consider that all the radiation is absorbed by the external walls. This case is denominated as radiation to ambient, and a simple formula for the corresponding thermal resistance R_{rad} in (6), compatible with the conduction and convection thermal network, can be extracted. The concept of heat transfer coefficient can be applied as in (5), where h_{rad} depends on the emissivity of the surface material ε, the surface area A, the Stephan Boltzmann's constant σ, the surface temperature T_s and the ambient temperature T_∞

$$q = h_{\text{rad}} A\Delta T = \varepsilon\sigma A\left(T_\infty^4 - T_s^4\right) \tag{5}$$

$$R_{rad} = \frac{1}{h_{\text{rad}} A}. \tag{6}$$

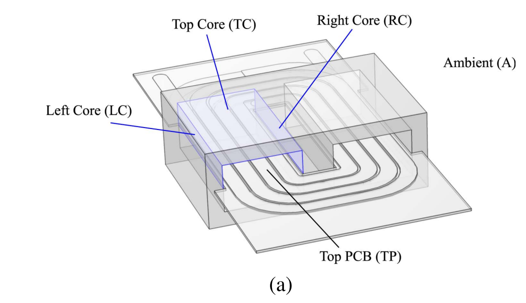

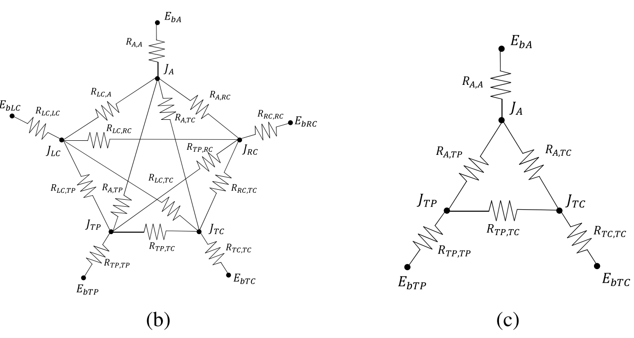

Fig. 2. Representation of radiation between surfaces. (a) Surfaces of the core considered for radiation between core and PCB. (b) Complete radiation network for the case depicted in (a). (c) Simplified radiation network.

In the case of a magnetic component, this expression is valid when the window is completely filled with the windings and insulation and there is no part of the winding considerably exceeding the width of the core, but for low utilization factors the interaction between surfaces is not negligible.

The approach of this work is illustrated in Fig. 2. As shown in Fig. 2(a), the top layer of the PCB is facing three of the inner surfaces of the core, marked in blue. The part of the windings which extends outside the core also interacts with the outer vertical faces, but will be neglected due to lower impact.

The radiation network for the considered surfaces is built as in Fig. 2(b), where the subscripts correspond to the ones indicated in Fig. 2(a). The external walls are large relative to the rest of surfaces and therefore considered as a blackbody (emissivity is equal to unity [16]) at ambient temperature.

At the nodes, J_i is the radiosity of each surface and E_{bi} is the emissive power of the surface if considered as a blackbody. To account for the real emissive power of the surfaces, the surface radiative resistances $R_{i,i}$ are added, which can be calculated based on the emissivity of the material and the area of the surface as in (7). The exchange between surfaces is represented by the space geometrical resistances $R_{i,j}$, which depend on the surface area and the view factor F_{ij} as in (8)

$$R_{i,i} = \frac{1-\varepsilon_i}{\varepsilon_i A_i} \tag{7}$$

$$R_{i,j} = \frac{1}{A_i F_{ij}}. \tag{8}$$

The height of the air space is generally small, so the view factor between the top PCB layer and the core parallel surface is larger than the view factor of orthogonal faces. Moreover,

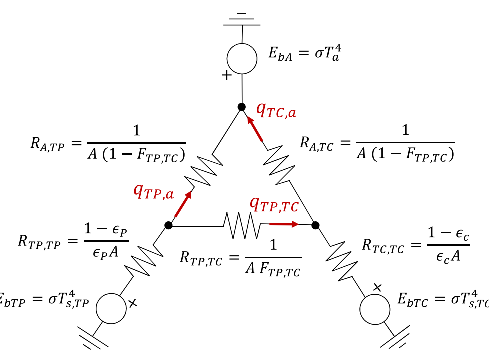

Fig. 3. Radiation network considered for the radiation between core and PCB inside the window. The arrows represent the heat transfer rates between nodes.

the core surfaces are connected by relatively low conduction resistance paths. These considerations make it reasonable to neglect the participation of vertical faces and only consider the radiation between top PCB layer, top window surface, and ambient. This simplification results in the network of Fig. 2(c), where the "Left Core" and "Right Core" surfaces have been removed.

For the exceeding winding surface (not covered by the core), together with the rest of the component surfaces in contact with the ambient, only radiation to ambient is considered and calculated following (5).

Since the sum of the view factors assigned to one surface must be the unity, the network can be reduced to the one in Fig. 3, where it is only needed to calculate one view factor before solving. From this network, the heat transfer rate between the two surfaces and ambient is obtained, and used to calculate the thermal resistances of (9)–(11), which are compatible with the general network

$$R_{rad,TP-TC} = (T_{s,TP} - T_{s,TC})/q_{TP,TC} \tag{9}$$

$$R_{rad,TP-a} = (T_{s,TP} - T_a)/q_{TP,a} \tag{10}$$

$$R_{rad,TC-a} = (T_{s,TC} - T_a)/q_{TC,a} \tag{11}$$

where $T_{s,i}$ are the temperatures of the considered surfaces and $q_{i,j}$ are the heat transfer rates between nodes.

D. Vertical Surfaces

When a magnetic core is present, the "thin plate" assumption presented in Section I becomes invalid. The vertical surfaces of the core must be considered for both convection and radiation.

The inner vertical surfaces can still be neglected for radiation, as aforementioned. The air space between core and winding, if it exists, will be generally small, so these surfaces may also be neglected for convection, following the same reasoning as for radiation.

Regarding the vertical outer surfaces, they must be considered for both mechanisms. This is done by finding the nodes in each plane belonging to each outer surface. Then the convection and radiation resistances are calculated following the same procedure as described for the nodes in horizontal surfaces.

III. Power Loss in Magnetic Components

In order to analyze the temperature rise under certain operating conditions, the losses generated inside the component must be calculated. In magnetic components, the frequency is usually pushed higher to shrink the size, which intensifies the appearance of eddy currents, greatly impacting the losses.

The accuracy of the results of the thermal model is affected by the accuracy in loss calculation. Since the focus of this work is to validate the thermal model, the applied loss model is kept simple, while considering the effect of high frequency and winding arrangement.

A. Core Loss Calculation

The Steinmetz equation [20] shown in (12) is extensively used to calculate the losses in the core under sinusoidal excitation. The coefficients of the formula can be found in the materials datasheet or derived from the volumetric loss curves provided by the manufacturer. These coefficients are sensitive to frequency and temperature, so it is recommended to characterize the material for the desired range of operation

$$P_{fe} = V_c K_c f^{\alpha} B_{\max}^{\alpha}. \tag{12}$$

For an adequate analysis of the accuracy of the thermal model, the uncertainty in loss calculation must be minimized. Hence, sinusoidal excitation is used in this work, allowing to apply (12) for core loss calculation.

Nevertheless, for nonsinusoidal excitation other models can be implemented, such as the improved generalized Steinmetz equation [20]. Other approaches involving machine learning and experimental based databases [21] can be used to improve the accuracy.

B. Copper Loss Calculation

Dowell's formula is popular for winding loss calculation [22] although only valid if the 1-D assumption is valid (high magnetizing inductance, no air gap, etc.). In [23], a derivation from Dowell's formula is obtained for different excitation waveforms and in [24] proximity losses are calculated based on the approximate average magnetic field between winding layers, providing (13) for multilayer foil conductors

$$P = R_{dc}\left(F_F \hat{I}^2 N + G_F \sum_{m=1}^{N} \hat{H}_{\text{avg}}^2\right) l_m. \tag{13}$$

This method loses accuracy when a large portion of the windings is not enclosed by the core or when the horizontal clearances are large. It is also not adequate if windings are close to an air gap, since the local fringing in the magnetic field cannot be analyzed with the 1-D approach. In [25] and [26], expressions for the fringing field due to an air gap and the generated losses in a copper turn depending on its location in space are presented.

In this work, (13) is used, adapted to PCB windings, since it enables to differentiate the losses in each layer due to high frequency effects and winding arrangement. However, for components where the 1-D approximation is not applicable, the 2-D

magnetic field should be accurately calculated either analytically or with FE simulations.

According to the power loss uniformity assumption in Section I, the total loss of each layer is divided into the total volume of copper in the layer. No distinction is made between turns inside the same layer.

As mentioned before, sinusoidal waveforms are used for verification. Nevertheless, this model can be used for loss calculation due to nonsinusoidal waveforms. In this case, the fast Fourier transform (FFT) of the waveform must be first obtained, the most relevant harmonics are selected and losses are calculated for each of the frequencies. The total loss is obtained by superposition.

C. Temperature Influence

Some of the materials properties vary with temperature, which makes the loss generation also temperature dependent. An electrothermal coupling can be added similarly to [11], [12] by adding an extra iterative process to modify these properties.

The proposed model studies the steady state of the component, where the operating conditions do not change. However, the material permeability is affected with temperature, which modifies the excitation of the core. If the information of permeability variation with temperature is available, it is used to update the value of the magnetic flux density. The Steinmetz coefficients can be adjusted with temperature, although this information is rarely provided by manufacturers, so most of the times a characterization of the material is needed.

Regarding the windings, the variation of copper conductivity affects the loss generation in two manners. On one hand, the dc resistance increases with temperature, due to inversely proportional relation with conductivity (14). However, the skin depth becomes thicker with lower conductivity, so the current distribution in the cross-sectional area of the wire may become more uniform. Thus, even if the frequency of operation does not change, the ratio between ac and dc current does vary with temperature

$$R_{dc,T} = \frac{L}{\sigma_T A} \tag{14}$$

$$P_{Cu,T} = \left.\frac{R_{ac}}{R_{dc}}\right|_T R_{dc,T} I_{\mathrm{rms}}^2$$

$$P_{Cu,(T+\Delta T)} \neq P_{Cu,T}\frac{\sigma_T}{\sigma_{(T+\Delta T)}}. \tag{15}$$

In (15), $P_{Cu,T}$ is the winding loss at temperature T, ΔT is the temperature increment, R_{ac}, R_{dc} are the ac and dc resistances of the wire, respectively, σ_T is the conductivity of copper at temperature T and I_{rms} is the RMS current through the winding. The error incurred by only adjusting the dc resistance and keeping the ac/dc ratio constant can be higher than the error of not considering the temperature variation, especially when the copper thickness is smaller than twice the skin depth at ambient temperature.

IV. Model Assembly and Solution

In a thermal network, only the most relevant heat transfer paths are taken into account and analyzed as a 1-D problem. When a 2-D or 3-D nature of heat transfer is considered, the possible approaches are to find an exact solution of the heat transfer equation (16), search in literature for shape factors, which can describe the system, or discretize the problem to apply finite element or finite difference solutions

$$\frac{\partial}{\partial x}\left(k\frac{\partial T}{\partial x}\right) + \frac{\partial}{\partial y}\left(k\frac{\partial T}{\partial y}\right) + \frac{\partial}{\partial z}\left(k\frac{\partial T}{\partial z}\right) + \dot{q} = \rho c_p \frac{\delta T}{\delta t}. \tag{16}$$

The finite difference method (FDM) approximates the heat equation to remove the derivative terms, resulting in a mesh where the nodes are connected in two directions through thermal resistances, which can be calculated equivalently to thermal networks [16], [17]. The drawback of discretized methods is that the accuracy of the results depend on the mesh resolution. If high accuracy is needed, a large number of nodes is required, which increases computation time and complexity to build the model, especially in a 3-D approach. The proposed model is based on the FDM, where the assumptions explained in Section I are used to describe the winding geometry in high detail with reduced complexity.

The objective is to discretize the component into a mesh with nodes and obtain the equivalent circuit. The circuit is then modeled as a matricial system using the Nodes Solution Method commonly employed for electric networks. The matricial system is shown in (17), where P_i is the heat transfer rate, T_i is the temperature, Y_{ij} are the elements of the admittance network, and i, j are the indices of the nodes in the mesh

$$\begin{bmatrix} P_1 \\ P_2 \\ \vdots \\ P_n \end{bmatrix} = \begin{bmatrix} Y_{11} & Y_{12} & \cdots & Y_{1n} \\ Y_{21} & Y_{22} & \cdots & Y_{2n} \\ \vdots & \vdots & \ddots & \vdots \\ Y_{n1} & Y_{n2} & \cdots & Y_{nn} \end{bmatrix} \begin{bmatrix} T_1 \\ T_2 \\ \vdots \\ T_n \end{bmatrix} \tag{17}$$

$$Y_{ii} = \sum_i \frac{1}{R_{ij}} \tag{18}$$

$$Y_{ij} = -\frac{1}{R_{ij}}. \tag{19}$$

The use of the admittance matrix instead of the impedance matrix makes the addition of new nodes and connections very simple. The terms in the diagonal or self terms, Y_{ii} in (18), are the sum of all the admittances connected to each node, while the terms outside the diagonal or mutual terms, Y_{ij} in (19), are the admittances between the two nodes corresponding to the indices of the position, with negative sign. This way, every time a new resistance is calculated, it can be simply added to the existing value in the corresponding position, without modifying the rest of the matrix or changing its size.

Furthermore, since the resistances can be added independently, the matrices for conduction, convection, and radiation can be calculated separately and added together to form the total matrix. As a consequence, the conduction matrix, which does not depend on temperature, can be extracted from the iterative

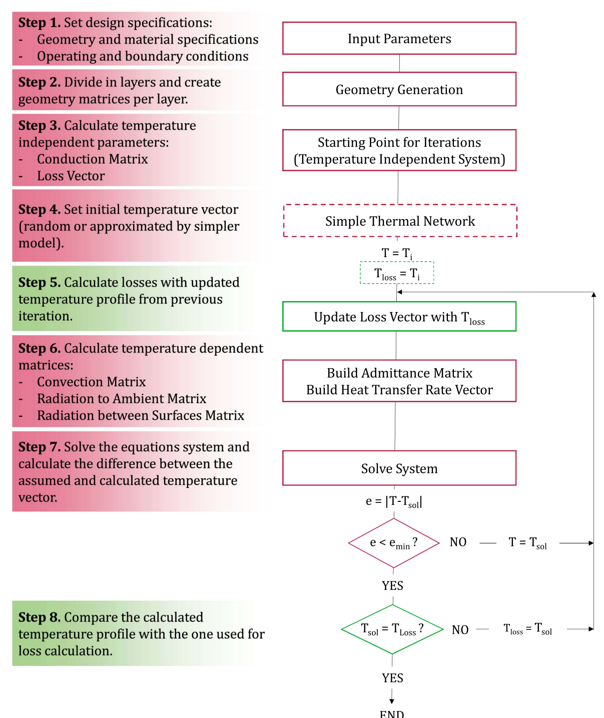

Fig. 4. Flowchart of the model definition and solution without (red) and with (red + green) electrothermal coupling.

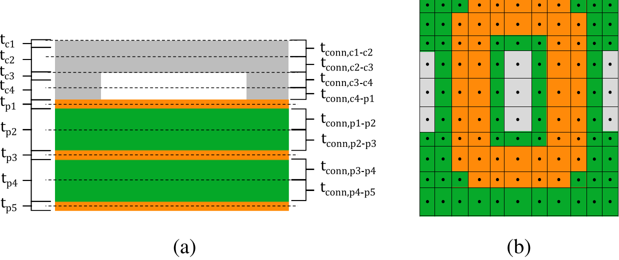

Fig. 5. Division of the component. (a) Representation of the cross section of a PCB with core and air space in the window, where the thicknesses considered for the thermal model are indicated. The dashed lines correspond to the modeled 2-D planes. The terms t_ci, t_pi are the thicknesses for the 2-D planes of core and PCB, respectively, and $t_{conn,i-j}$ are the thicknesses for vertical connection between planes. (b) Division of a copper layer in nodes, represented by dots.

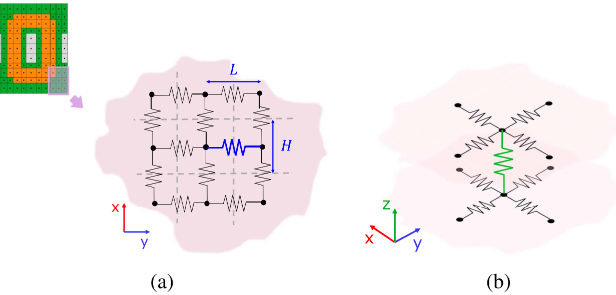

Fig. 6. Representation of the connection between nodes. (a) 2-D connection between nodes inside a layer. (b) 3-D connection between layers.

process as shown in Fig. 4, which improves the efficiency of the model.

A. Geometry of the Model

The flowchart in Fig. 4 resumes the steps of the model creation and solution. The *Geometry Generation* step consists on creating the set of matrices containing the information about dimensions, material properties, and boundary conditions according to the specifications.

The geometry matrices divide the component in layers. For simplicity, only the PCB windings will be initially considered. To accurately model the 3-D heat transfer, the model must contain at least one 2-D mesh for each copper layer and one 2-D mesh for each insulation layer, due to the large thermal conductivity difference. Therefore, if the winding is formed by a m-layer PCB, the total number of layers in the model will be $2m - 1$, m of them being copper layers and $m - 1$ being insulation layers. Each layer is considered then as a 2-D plane and divided into square elements.

B. Temperature Independent System

After generating the geometry, the initial loss vector and the conduction matrix can be calculated (step 3 in Fig. 4).

1) Conduction Matrix: The conduction matrix depends on the thermal conductivity of the solid materials and the dimensions. For the typical materials used in PCB magnetic components, the variation of thermal conductivity in the range of interest (approximately between 20 °C and 100 °C) is negligible. Regarding the dimensions, the coefficient of thermal expansion of copper and insulation is similar to avoid problems during PCB manufacture processes. Furthermore, the error associated with the change in dimensions due to manufacturer tolerances is higher than the maximum expansion of the considered materials in the range of interest. Hence, the conduction matrix can be considered constant with temperature, and it can be calculated out of the iterative loop.

The nodes of the mesh are connected in the two dimensions and the thermal resistances due to conduction are calculated according to (2) between each pair of nodes. The thickness of each layer is determined as in Fig. 5(a) to calculate the dimensions of each heat path. The 2-D meshes are centered in the corresponding layer, as shown in the left side of Fig. 5(a). The thickness of copper layers is considered for the 2-D plane resistance network, but neglected during 3-D assembly for simplicity, as shown in the right side of Fig. 5(a). This simplification is made based on the large difference between copper and insulation layers thickness and on the small temperature gradient in the vertical direction inside the copper tracks.

The thermal resistances are placed in the admittance matrix of (17), where i, j represents the nodes indices. The admittance matrix is a square matrix of size $n \times n$, being n the number of nodes. To complete the conduction admittance matrix, the layers are joined together. This means every node is connected to its equivalent in the adjacent layer through a conduction resistance.

The 2-D and 3-D connections between nodes are shown in Fig. 6. The dashed lines in Fig. 6(a) delimit the area of the plane

corresponding to each node. One resistance is highlighted in Fig. 6(a) for clarification: the length of the corresponding path is depicted as L and the cross-sectional area is the product of H by the depth of the plane. In the case of the 3-D connection, highlighted in Fig. 6(b), the length is the distance between layers and the cross-sectional area is delimited by the dashed lines in the 2-D plane. The element or unit cell of the model is the volume assigned to each node, which has the shape of an hexaedron.

2) Element Size: The size of the elements impacts both the accuracy and efficiency of the model. With a finer mesh, the discretization and linearization of the heat transfer equation will involve lower error, but the number of nodes to be computed will increase.

Despite the size of the matrix is generally large, the majority of terms are null, because each node is connected to a maximum of other six nodes, as can be inferred from Fig. 6(b). Thus, treating it as a sparse matrix can save memory during execution, making the model more efficient and enabling the creation of larger meshes. It is also possible to reduce the number of nodes by enabling different element size throughout the 2-D plane. However, to avoid compromising the simplicity of construction of the admittance matrix, all 2-D resistances must be restricted to the directions of the x and y axes, and every node in a 2-D plane must be aligned in the z-direction with the corresponding nodes in the adjacent planes. In consequence, all elements must be hexaedrons.

In order to find the optimal mesh for a specific device and a desired level of accuracy, a convergence study can be performed. This study is used in FE simulations and consists on starting the calculation with a very coarse mesh and then decreasing the element size step by step. After each step, the relative difference between the current solution and the previous one is calculated. Convergence is found when the difference reaches the maximum admissible value defined by the user.

3) Losses Vector: The losses are calculated according to the selected loss model. In this work, the model explained in Section III is applied.

In the thermal model, these losses are included as current sources, assigning the proportional fraction of loss to each node. These current injections are included in the corresponding positions of the loss vector.

If losses are considered independent from temperature, the *Loss Vector Calculation* step (step 5 in Fig. 4) can be extracted from the iterative process.

C. Temperature-Dependent Parameters

The iterative process involves steps 6 and 7 from Fig. 4. An initial temperature vector must be assumed. To reduce the number of iterations, this temperature profile may be approximated using a simple thermal network (step 4 in Fig. 4, marked with dashed lines to indicate that it is optional). Then, the temperature-dependent resistances are calculated according to the equations in Section II to *Build the Admittance Matrix* (step 6).

The ambient is modeled as a voltage source of value equal to the ambient temperature, connected to ground. Convection and radiation resistances are connected in parallel, since they both support heat dissipation to the ambient. This parallel resistance is connected in series to the voltage source. To solve the system with (17), the voltage sources with series resistances must be transformed to their equivalent parallel circuit with current sources. These currents are added to the loss vector to *Build the Heat Transfer Rate Vector* (step 6). The ground node shall not be included in the admittance matrix, thus the addition of these resistances only affects the values in the diagonal (self-terms).

The step *solve system* applies (17) to obtain the temperature vector. The error of the iteration step is calculated as the absolute difference between the assumed temperature vector and the calculated one. If the maximum error is higher than the admissible, the calculated vector is set as assumed vector for the next iteration and the process is repeated until convergence is reached.

D. Electrothermal Coupling

To contemplate the intrinsic relation between temperature and loss generation, the process is enclosed in another iterative process, which is marked in green color in Fig. 4. In step 5, the loss vector is updated considering the variation of materials properties explained in Section III-C.

Step 8 adds a second condition to detect convergence: the difference between the calculated temperature and the temperature used to evaluate the losses in the component must be sufficiently small.

V. Verification of the Model

The model has been verified with FE simulations in COMSOL Multiphysics and experimental measurements with thermal camera. In order to analyze the accuracy and limitations of the model, several designs of both inductors and transformers with different geometries and configurations have been tested.

Table I defines the characteristics of each of the inductor designs and Table II collects the transformer designs. These designs are combinations of three different PCB layouts with different number of turns and copper widths. All the boards have four layers, where the outer ones have a thickness of 1 oz and the inner ones have a thickness of 0.5 oz. For the designs with more than four layers, several boards have been stacked together, adding two layers of kapton tape between boards. The board thickness shown in the tables is the total thickness of the stack.

Experiments have been conducted with dc and ac excitations. In the case of ac excitation, sinusoidal currents have been used, varying both the amplitude and frequency, in a range between 40 and 240 kHz. In order to obtain different loss distributions between core and winding, the inductors have been tested with different gap lengths and the transformers have been tested with different loads. Regarding the cooling technique, natural and forced air convection have been used. All temperatures have been measured at steady state.

TABLE I
INDUCTOR VERIFICATION DESIGNS

	I-1	I-2	I-3	I-4	I-5	I-6	I-7	I-8	I-9	I-10
Inductance (μH)	552	240	552	240	552	240	390	170	390	170
Layers	4	4	8	8	12	12	4	4	16	16
Turns per layer	8/4/4/8	8/4/4/8	8/4/4/8 $\times 2$	8/4/4/8 $\times 2$	8/4/4/8 $\times 3$	8/4/4/8 $\times 3$	5/5/5/5	5/5/5/5	5/5/5/5 $\times 4$	5/5/5/5 $\times 4$
Gap (μm)	250	750	250	750	250	750	250	750	250	750
Board thickness (mm)	1.2	1.2	2.57	2.57	3.93	3.93	1.0	1.0	4.5	4.5
Track width (mm)	2/4/4/2	2/4/4/2	2/4/4/2	2/4/4/2	2/4/4/2	2/4/4/2	2.92	2.92	2.92	2.92

TABLE II
TRANSFORMER VERIFICATION DESIGNS

	T-1	T-2	T-3	T-4	T-5	T-6	T-7
Turns ratio	1:1	1:1	2:3	2:3	2:3	1:1	1:1
Primary layers	4	6	2	2	8	4	4
Primary turns/layer	8/4/4/8	8/4 ($\times 3$)	4/2	4/2	4/2 ($\times 4$)	5/5/5/5	5/5/5/5
Secondary layers	8	6	2	2	8	4	4
Secondary turns/layer	8/4/4/8 ($\times 2$)	8/4 ($\times 3$)	3/6	3/6	3/6 ($\times 4$)	5/5/5/5	5/5/5/5
Configuration	PPPP/SSSS/SSSS	PPSS ($\times 3$)	PPSS	PPSS	PPSS ($\times 4$)	PPPP/SSSS	PPPP/SSSS
Core	EE	EE	EI	EE	EE	EE	EI
Gap (μm)	250	250	167	250	250	250	167
Board thickness (mm)	3.93	3.93	1.6	1.6	6.9	2.17	2.17
Track width (mm)	2/4/4/2 ($\times 3$)	2/4/4/2 ($\times 3$)	1.65/3.5/2/1	1.65/3.5/2/1	1.65/3.5/2/1 ($\times 4$)	2.92	2.92

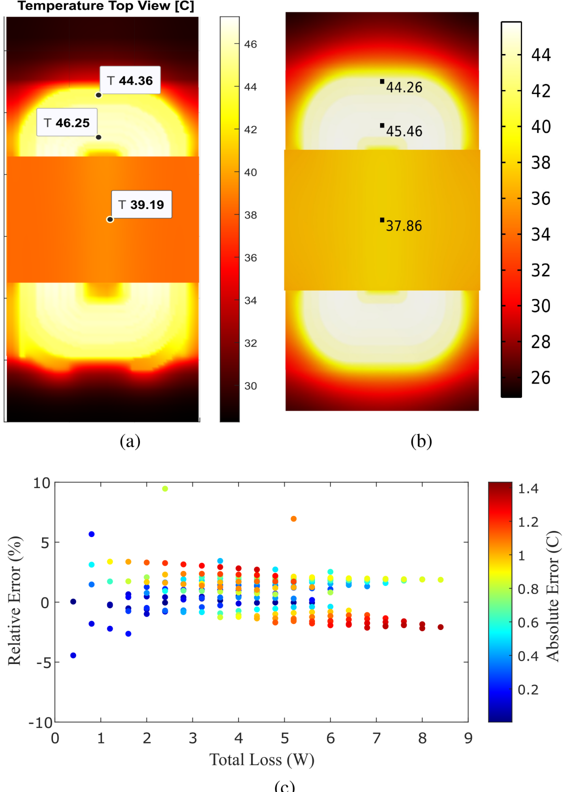

Fig. 7. Comparison of the temperature distribution of transformer T-1 from Table II obtained with (a) the proposed model and (b) COMSOL simulation, for natural convection and AC excitation. (c) Absolute and relative error respect to simulation for transformer T-1 for a power loss sweep varying both core and winding losses between 0 and 4.2 W, and applying natural convection and forced air convection at 3 m/s.

An example of the results can be observed in Figs. 7 and 8. In Fig. 7, the temperature profile obtained with the thermal model for one of the tested specimens is compared to the results obtained with a FE simulation, showing good agreement. In Fig. 7(c), the error of the model taking the simulation as reference is plotted for a set of simulations varying the losses in both the core and the winding. This parametric analysis has been performed for both natural and forced air convection, plotting the results together in the graph. The maximum absolute error is 1.4 °C and most results are contained within a ±5% range of relative error.

Fig. 8 illustrates the comparison between the proposed model results and experimental measurement for one of the tested designs. For a complete validation of the model, the results have been analyzed in terms of accuracy and time consumption. This study has revealed the benefits and limitations of the model, which are detailed in this section.

A. Accuracy Analysis

For each of the experiments, at least one measurement of the core and one measurement of the PCB (typically the hot spots) have been compared to the calculated values. The obtained errors for the dc and ac tests are shown in Figs. 9 and 10, respectively. The absolute error is the difference between calculated and measured temperature, while the relative error is the percentage difference, referred to the measured temperature increase with respect to the ambient temperature.

The maximum error obtained in the dc tests is 4 °C, being approximately a 92% of the results in the sample contained within ± 3.2 °C of absolute error. In the ac tests, this 92% range expands to ± 3.5 °C of absolute error or ± 12% of relative error. This detriment in accuracy was expected due to the added uncertainty in the loss calculation. As the losses in the device are not measured, but calculated or simulated with FE software, there is an added error due to the impact of eddy currents in the experiments with ac excitation.

On the other hand, the accuracy of the devices used for measurement must be taken into account. For the measurement of the temperatures, a thermal camera Fluke Ti-400 with accuracy of ± 2 °C (or ± 2% of the measurement, whichever is the largest)

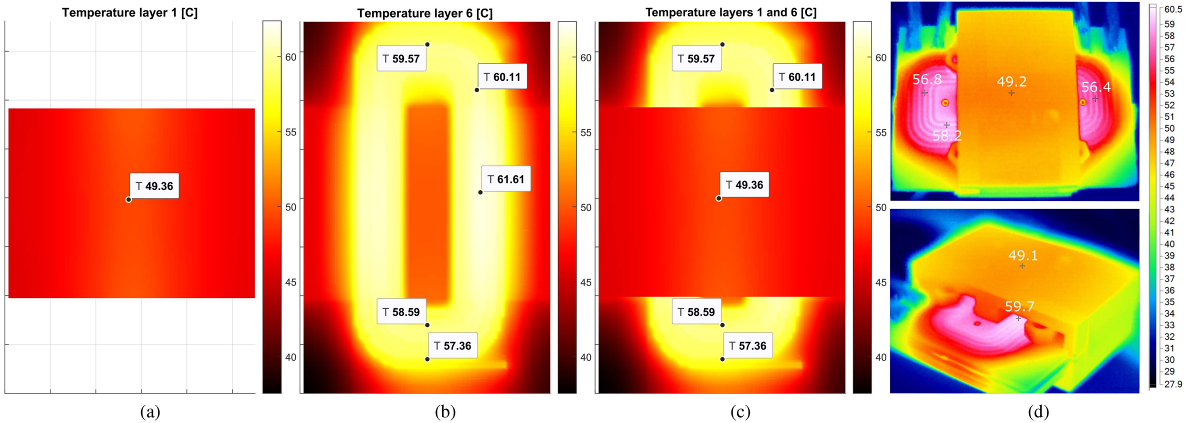

Fig. 8. Example of the results obtained with the thermal model for the transformer T-5 from Table II with natural convection and AC excitation. Temperature distribution obtained with the model for (a) top core layer; (b) top PCB layer; (c) top view of the transformer; and (d) measured temperature with thermal camera.

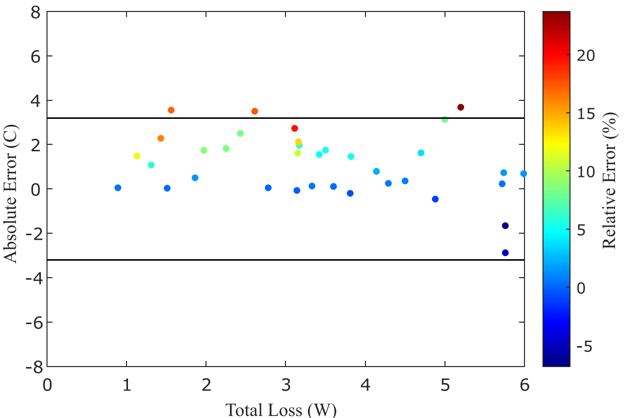

Fig. 9. Errors obtained in the experiments with DC excitation, respect to total loss in the device. The horizontal lines represent the error limits where approximately 92% of the results are contained.

TABLE III
COMPARISON WITH EXISTING MODELS

Reference	[5]	[6]	[7]	[9]	Proposed
M/S req.[a]	Yes	Yes	No	No	No
Average error (°C)	3.27	1.1	2.5	1.9	1.68 (1.28[b])
Maximum error (°C)	6	1.2	5.1	3.7	3.5[b]
Average error (%)	15.4	19.9	11	3.5	6.37 (4.56[b])
Maximum error (%)	43.3	24.5	56	7.8	12[b]
Sample size[c]	10	1	12	1	67

[a]Measurement or Simulation used for thermal impedance calculation.
[b]Considering 92% of the results, as explained in Section V-B.
[c]Number of results used to calculate the error.

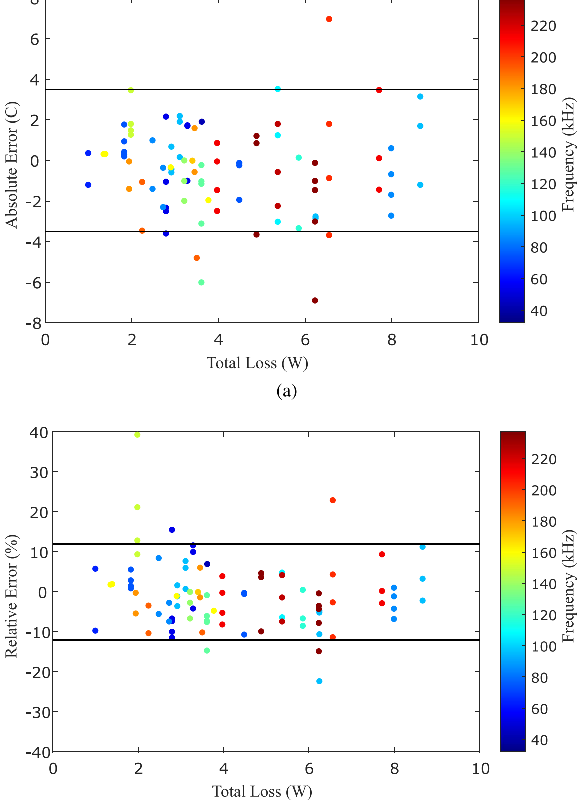

Fig. 10. Errors obtained in the experiments with AC excitation, respect to total loss in the device and frequency of the excitation. The horizontal lines represent the error limits where approximately 92% of the results are contained. (a) Absolute error in degrees. (b) Relative error in percentage of the measured temperature increment.

and thermal contacts with accuracy of ± 0.2 °C have been used. For the air flow speed, an anemometer RS-8880 with accuracy of ± (0.01 m/s + 5% reading) is used. Regarding the electrical measurement equipment, the current probes RT-ZC20B have an attenuation of 10:1 with attenuation error of 2% of the measurement, and the voltage probes RT-ZD01 have an attenuation of 100:1 with attenuation error of 2%.

The presented model has been validated with a large sample of designs and operating conditions, which is not found in the literature for other existing models. A comparison among models documented in the state of the art is shown in Table III in terms of accuracy, according to the published results. Considering both absolute and relative errors, the proposed model predicts the temperature better than state-of the art thermal networks, even the ones using measurement or simulation-based parameters. The model in [9] claims superior accuracy, although results are shown for only one specific case, comparison is made with FE and time consumption is not evaluated.

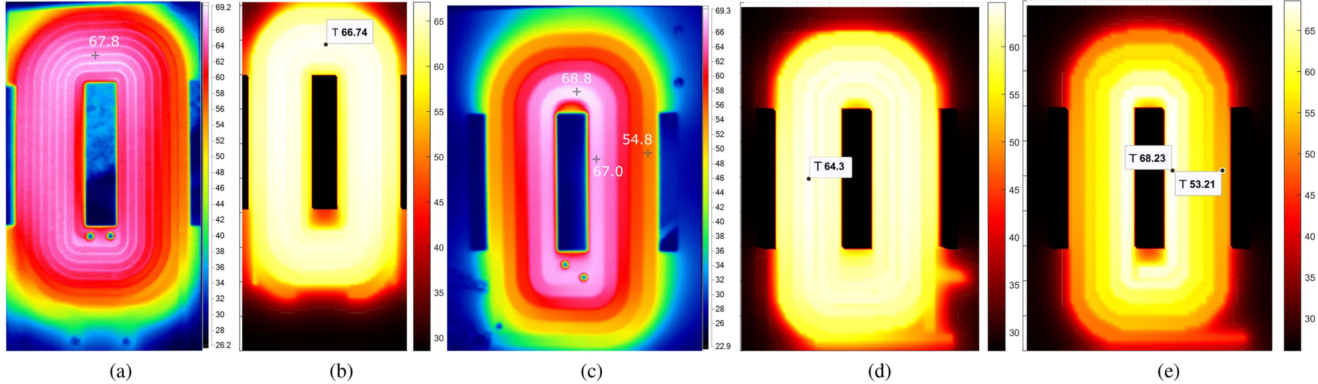

Fig. 11. Limitation of the "loss uniformity per layer" assumption (all scales in °C). Inductors I-1 and I-7 from Table I without core are compared under excitation of 2 A at 130 and 140 kHz, respectively. The tests are performed with natural convection at 27 °C ambient temperature. Inductor I-1: (a) thermal camera; (b) proposed model; Inductor I-7: (c) thermal camera; (d) proposed model; (e) proposed model with added differentiation of losses per turn.

B. Limitations of the Model

The losses calculation described in Section III has been successfully applied to the thermal model for the transformer designs. However, in the case of inductors, the impact of the gap and the orthogonal magnetic fields in the spaces between core and winding when the separation between them is too large, lead to deviation from the errors shown in Fig. 10. For this reason, in this work, the losses applied to the inductor models are obtained from FE simulation, instead of analytical calculation, since the main goal of this article is the thermal model itself and its validation. In further research, the effect of the air gap will be included in the analytical calculation to avoid the need for FE simulations.

The results of the experiments also revealed that the loss uniformity assumption presented in Section I cannot be always applied, as its accuracy strongly depends on the winding configuration. In fact, the results exceeding the error ranges depicted in Fig. 10 are caused by this assumption. To illustrate this phenomenon, Fig. 11 depicts two of the inductor designs excited at similar frequencies and the temperature distribution obtained with thermal camera and with the model for the top layer of the PCB. The core has been removed for more clarity in the picture.

While the temperature rise in the case of Fig. 11(a) is accurately predicted by the model, the one in Fig. 11(c) shows a much less uniform profile in reality than in the prediction, leading to an error of 4 °C in the hot spot. If the losses are differentiated not only per layer, but per turn, the temperature distribution of Fig. 11(e) results, which is more similar to the real one, having an error of less than 1 °C in the hot spot.

The differentiation of losses per turn cannot be performed using the loss model described in Section III, since the magnetic field inside each layer is considered uniform. Therefore, the loss calculation must be improved for cases where the magnetic field distribution inside the layer is highly nonuniform.

C. Time Consumption

The proposed thermal model presents an accuracy close to FE simulations with purely analytical calculations, with the main limitation of achieving an accurate calculation of losses. However, the computation time is shorter than in simulation.

TABLE IV
COMPUTATION TIME COMPARISON

Method	Proposed	FE - Solids[a]	FE - CFD[b]
Average time per node (ms)	0.18	2.2	4.2
Max. time per node (ms)	0.20	2.7	5.8

[a]Using correlations for h coefficients.
[b]Heat Transfer coupled with Fluid Dynamics.

To perform a speed comparison between the model and FE simulation, the total time consumption divided by the number of nodes has been evaluated. The results are presented in Table IV. In this table, two types of simulation are considered. The more accurate simulation computes the fluid dynamics in the air domain. The faster simulation uses correlations to evaluate the heat transfer coefficient at the surfaces. The version 5.6 of COMSOL Multiphysics has been used for the FE simulations.

The number of nodes of the analyzed cases varies between $3{\cdot}10^4$ and 10^5 for the solid parts (up to $4.5{\cdot}10^5$ including the air domain) and has been kept similar between model and simulation for both accuracy and time comparison. The results show that the proposed model is approximately 13 times faster than the simplified simulation.

VI. CONCLUSION

A thermal model has been proposed, which is suitable for PCB magnetic component optimization. The model accuracy is comparable to finite element software, while the computation time is reduced to approximately 13 times the time spent in FE simulation. Moreover, the model consists of iterative assembling and solution of a matrix system, which makes possible to implement it in open source software tools.

The fundamentals and parameters needed to build the model have been presented, as well as the solution. The basic model comprises the loss calculation and an iterative process to calculate the temperature rise. To improve the accuracy, the dependence of the materials properties with temperature is considered

by adding another iteration loop to link temperature and loss calculation.

Design examples have been built and tested to verify the proposed model for air cooling conditions, both with natural and forced flow. The validation has been done with 17 samples and 67 tests, which represents an intensive testing campaign compared to the published results in literature. Tests have been conducted with dc and ac excitation, revealing the limitations of the model when eddy currents appear.

The model is specifically developed for PCB magnetic components, due to simplifications performed based on the assumptions of Section I. The concept, however, can be applied to other types of magnetic components, with the expense of either higher complexity or lower accuracy. It can also be used to analyze the thermal behavior of other PCB components.

The model will be used in future research work to investigate the limitations of PCB magnetic components for high power applications. The benefits of integrating the thermal model in design optimization processes will be explored. The limitations of the model in terms of loss calculation will also be addressed in future research.

References

[1] E. M. Dede et al., "Thermal design, optimization, and packaging of planar magnetic components," *IEEE Trans. Compon. Packag. Manuf. Technol.*, vol. 11, no. 9, pp. 1480–1488, Sep. 2021.

[2] L. M. Escribano, P. Zumel, R. Prieto, J. A. Oliver, and J. A. Cobos, "A very simple analytical approach of thermal modeling for magnetic components," in *Proc. IEEE 20th Annu. Appl. Power Electron. Conf. Expo.*, 2005, pp. 1944–1950.

[3] J. Adam, "New correlations between electrical current and temperature rise in PCB traces," in *Proc. IEEE 20th Annu. Semicond. Thermal Meas. Manage. Symp.*2004, pp. 292–299.

[4] M. C. Smit, J. A. Ferreira, J. D. van Wyk, and M. Ehsani, "Technology for manufacture of integrated planar LC structures for power electronic applications," in *Proc. IEEE 5th Eur. Conf. Power Electron. Appl.*, 1993, pp. 173–178.

[5] M. Rascon, J. Ara, R. Madsen, J. Navas, M. Perez, and F. San Miguel, "Thermal analysis and modelling of planar magnetic components," in *Proc. IEEE 16th Annu. Appl. Power Electron. Conf. Expo.*,2001, pp. 97–101.

[6] Z. Shen, Y. Shen, B. Liu, and H. Wang, "Thermal coupling and network modeling for planar transformers," in *Proc. IEEE Energy Convers. Congr. Expo.*, 2018, pp. 3527–3533.

[7] A. Lewaiter and B. Ackermann, "A thermal model for planar transformers," in *Proc. IEEE 4th Int. Conf. Power Electron. Drive Syst.*, 2001, pp. 669–673.

[8] M. Mogorovic and D. Dujic, "Thermal modeling and experimental verification of an air cooled medium frequency transformer," in *Proc. IEEE 19th Eur. Conf. Power Electron. Appl.*, 2017, pp. P.1–P.9.

[9] R. Shafaei, M. Ordonez, and M. A. Saket, "Three-dimensional frequency-dependent thermal model for planar transformers in LLC resonant converters," *IEEE Trans. Power Electron.*, vol. 34, no. 5, pp. 4641–4655, May 2019.

[10] R. Wrobel and P. H. Mellor, "A general cuboidal element for three-dimensional thermal modelling," *IEEE Trans. Magn.*, vol. 46, no. 8, pp. 3197–3200, Aug. 2010.

[11] K. Nakamura, H. Yoshida, and O. Ichinokura, "Electromagnetic and thermal coupled analysis of ferrite orthogonal-core based on three-dimensional reluctance and thermal-resistance network model," *IEEE Trans. Magn.*, vol. 40, no. 4, pp. 2050–2052, Jul. 2004.

[12] M. Stojadinović and J. Biela, "Modeling and design of a medium-frequency transformer for high-power dc-dc converters," *IEEJ J. Ind. Appl.*, vol. 8, no. 4, pp. 685–693, 2019.

[13] G. S. López, A. D. Expósito, J. Munoz-Anton, J. Á. O. Ramírez, and R. P. López, "Fast and accurate thermal modeling of magnetic components by FEA-based homogenization," *IEEE Trans. Power Electron.*, vol. 35, no. 2, pp. 1830–1844, Feb. 2020.

[14] V. Bissuel et al., "Novel approach to the extraction of Delphi-like boundary-condition-independent compact thermal models of planar transformer devices," in *Proc. IEEE 24rd Int. Workshop Thermal Investigations ICs Syst.*,2018, pp. 1–7.

[15] L. C. Ordonez, A. D. Exposito, P. A. Cervera, M. Bakic, and T. Wijekoon, "Optimized thermal modelling of high power planar PCB magnetics," in *Proc. IEEE Energy Convers. Congr. Expo.*, 2022, pp. 1–8.

[16] F. P. Incropera et al., *Fundamentals of Heat and Mass Transfer*, vol. 6. New York, NY, USA: Wiley, 1996.

[17] Y. Cengel, *Heat Transfer A Practical Approach*, 2nd ed., McGraw-Hill, 2003.

[18] K. Górecki, K. Detka, and K. Górski, "Compact thermal model of the pulse transformer taking into account nonlinearity of heat transfer," *Energies*, vol. 13, no. 11, 2020, Art. no. 2766.

[19] M. Mikha-Beyranvand, J. Faiz, B. Rezaeealam, A. Rezaei-Zare, and M. Jafarboland, "Thermal analysis of power transformers under unbalanced supply voltage," *IET Elect. Power Appl.*, vol. 13, no. 4, pp. 503–512, 2019.

[20] W. G. Hurley and W. H. Wölfle, *Transformers and Inductors for Power Electronics: Theory, Design and Applications*. Hoboken, NJ, USA: Wiley, 2013.

[21] H. Li et al., "MagNet: An open-source database for data-driven magnetic core loss modeling," in *Proc. IEEE Appl. Power Electron. Conf. Expo.* 2022, pp. 588–595.

[22] P. Dowell, "Effects of eddy currents in transformer windings," *Proc. Inst. Elect. Engineers*, vol. 113, no. 8, , pp. 1387–1394, 1966.

[23] W. G. Hurley, E. Gath, and J. G. Breslin, "Optimizing the AC resistance of multilayer transformer windings with arbitrary current waveforms," *IEEE Trans. Power Electron.*, vol. 15, no. 2, pp. 369–376, Mar. 2000.

[24] J. Mühlethaler, "Modeling and multi-objective optimization of inductive power components," Ph.D. dissertation, ETH Zurich, Zürich, Switzerland, 2012.

[25] W. A. Roshen, "Fringing field formulas and winding loss due to an air gap," *IEEE Trans. Magn.*, vol. 43, no. 8, pp. 3387–3394, Aug. 2007.

[26] P. Wallmeier, "Improved analytical modeling of conductive losses in gapped high-frequency inductors," *IEEE Trans. Ind. Appl.*, vol. 37, no. 4, pp. 1045–1054, Jul./Aug. 2001.

Lucia Clavero Ordonez (Graduate Student Member, IEEE) received the B.Sc. degree in mechanical and electrical engineering from the Universidad de Málaga, Málaga, Spain, in 2018, and the M.Sc. degree in industrial engineering from the Universidad Politécnica de Madrid (UPM), Madrid, Spain, in 2020. She is currently working toward the industrial Ph.D. degree in electronic engineering with UPM and the Research Center of Huawei in Nuremberg, Germany.

Her research interests include modeling and optimization of high frequency magnetic components, thermal modeling for PCB components and power density improvement for isolated ac/dc converters.

Alberto Delgado Exposito (Member, IEEE) received the B.Sc. degree in electrical engineering from the University of Málaga (UMA), Málaga, Spain, in 2016 and the M.Sc. and Ph.D. degrees in industrial electronics from the Universidad Politécnica de Madrid (UPM), Madrid, Spain, in 2017 and 2021, respectively.

During his undergraduate studies, he was awarded honors on several occasions, and he achieved the Best Student of the Year Award. He is currently a Assistant Professor at UPM. His research activities include modeling of dc–dc converters for inductive power transfer system, high-frequency magnetic components for different applications, and nano and micromagnetic materials.

Pedro Alou Cervera (Member, IEEE) was born in Madrid, Spain, in 1970. He received the M.S. and Ph.D. degrees in electrical engineering from the Universidad Politécnica de Madrid (UPM), Madrid, Spain, in 1995 and 2004, respectively.

He is currently a Full Professor and participates in the management of the UPM as a Deputy Vice Chancellor. He has been involved in Power Electronics since 1995, participating in more than 70 R&D projects with the industry. He has authored or coauthored more than 50 journal articles, 150 conference papers, and holds six patents. His main research interests are in power converters, advanced topologies for efficient energy conversion, modeling of converters and magnetic components, advanced control techniques for high dynamic response, energy management and new semiconductor technologies for power electronics. His research activity is distributed among industrial, aerospace, and military projects.

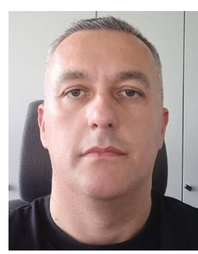

Miroljub Bakic received the Dipl.-Ing. degree in electrical engineering from the University of Belgrade, Belgrade, Serbia, in 2007.

He was with TPP Nikola Tesla A and the Nikola Tesla Institute of Electrical Engineering, Belgrade, until 2012 working on converter design for electrostatic precipitators and generator excitation units. Since 2012, he has been with Huawei Technologies, NRC, Nuremberg, Germany, currently as a Senior Design Engineer. His current research interests include power electronics, uninterruptible power supplies, and solar inverters with main focus on magnetic component design.

Thiwanka Wijekoon (Senior Member, IEEE) received the B.Sc. (Hons.) degree in electrical and electronic engineering from the University of Peradeniya, Sri Lanka, in 2001 and the Ph.D. degree in power electronics from the University of Nottingham, Nottingham, U.K., in 2006.

He is currently the Leader of the Power Electronics Technology R&D Group responsible for next generation converter designs for Solar & UPS applications at Huawei's Nuremberg Research Center in Germany since 2016. He was a Lecturer in electrical and information engineering with the University of Ruhuna, Sri Lanka, until 2005. From 2006 to 2010, he has been a Postdoctoral Research Fellow with the PEMC Group, University of Nottingham working on multilevel power converters for more electric aircraft technology in collaboration with GE Aviation. In 2010, he joined GE Global Research-Europe as a Lead Research Engineer in the High Power Electronics Lab, working on large power converters for drives in O&G processing, MVDC transmission systems, Subsea electrification, Solar and DFIG wind converters. His current research interests include power-electronic converter topologies, modulation, control, WBG based design of converter systems for applications in Solar PV, Data Center and EV. He holds more than 21 granted patents to date and 50 more patent applications pending as well as coauthored more than 30 technical papers.